Oxide overlayer formation on sputtered ScAlN film exposed to air

Minghua Li,[a] Huamao Lin, Kan Hu, and Yao Zhu

AFFILIATIONS

Institute of Microelectronics, Agency for Science, Technology and Research (A*STAR), Singapore 138046, Singapore

Note: This paper is part of the APL Special Collection on Piezoelectric Thin Films for MEMS.
[a]**Author to whom correspondence should be addressed:** li_minghua@ime.a-star.edu.sg

ABSTRACT

There has been much interest in developing scandium doped aluminum nitride (ScAlN) thin films for use in electronic devices, due to their excellent piezoMEMS response, large spontaneous polarization, and the capability for CMOS-compatible integration. As with the undoped AlN film, the formation of an oxide overlayer on the air-exposed ScAlN film can modulate its surface structure and the electrical properties. In this study, we investigate the effects of surface oxidation on a ScAlN film by characterizing the film microstructure and the elemental chemical states. We found that amorphous phase and small crystallites co-exist in the oxide overlayer, which is remarkably different from the columnar (0002) crystalline texture in the bulk ScAlN film. X-ray photoelectron spectroscopy core-level analyses confirm the formation of Al–O and Sc–O bonds. Moreover, the valence band maximum of the oxide overlayer shifts toward a higher binding energy, indicating a high energy barrier at the ScAlN/metal interface. Our results suggest that ScAlN surface oxidation is a chemical reaction-driven and self-limited process.

 https://doi.org/10.1063/5.0106717

Scandium doping greatly enhances the piezoelectric response in aluminum nitride (ScAlN) thin films. This has led to much interest in developing ScAlN-based electronic devices.[1–3] Even so, there are challenges in design and fabrication of such films, as the dielectric and piezoelectric behaviors are very sensitive to Sc doping concentration,[4] crystallographic orientation,[5] stress,[6] nonstoichiometric vacancies,[7] and foreign impurities like oxygen.[8]

Even though AlN and ScAlN films are thermally robust, the bulk films maintaining their Wurtzite structure after annealing at temperature up to 1000 °C,[9–11] their chemical stability remains a concern. Surface oxidation has been reported on AlN films deposited using magnetron sputtering,[12] pulse laser deposition,[13] and atomic layer deposition.[14] This oxidation causes the decrease in piezoelectric modulus d_{33} of a sputtered AlN film.[15] It also impacts the reliability of piezoelectric devices, with such oxidation in an AlN-based surface acoustic wave device increasing insertion loss and operating frequency drift.[16] Oxidation of AlN films is a chemical reaction controlled process,[17] with reaction kinetics strongly influenced by temperature, oxygen partial pressure, humidity, and film surface structure.[18] Epitaxial growth of the oxide overlayer was found on a single crystalline AlN annealed at 1000 °C.[19] Another study[20] found that the N vacancy (V_N) formation accelerates the AlN oxidation reaction.

Oxidation on ScAlN film surfaces has also been studied on a ∼4 nm amorphous $(AlSc)_xO_y$ layer on a ∼20 nm $Al_{0.64}Sc_{0.36}N$ film surface.[21] With this oxide overlayer, the ferroelectric ScAlN film was found to be switchable, but other effects of the oxide overlayer remain unreported.[22,23] In this study, we used reactive sputtering to deposit a ScAlN film and allowed it to oxidize in a cleanroom environment. The oxidation reaction and the impacts of the oxide overlayer on the film surface morphology and electronic structure were then investigated.

The sample was prepared using a multi-chamber sputtering system, consisting of one DC and one reactive pulsed DC magnetron sputtering chamber. A ScAl alloy target contained 20 at. % of Sc was installed in the chamber with the pulsed DC power supply. A 200 mm Si (100) wafer was used as substrate. First, a 20 nm of AlN was reactively sputtered as seed layer to promote the crystallinity of the films grown on it. Next, a 200 nm of molybdenum (Mo) bottom electrode was deposited in the DC sputtering chamber. Without vacuum breaking, the wafer was then transferred to the reactive pulsed DC magnetron chamber for 1 μm thick ScAlN film deposition. Ar and N_2 were used as discharge and reactive gases for the reactive sputtering. No substrate heat was applied during the ScAlN deposition. Before being unloaded and exposed to air, the wafer was kept in vacuum to ensure its temperature reached room temperature. The sample was stored in

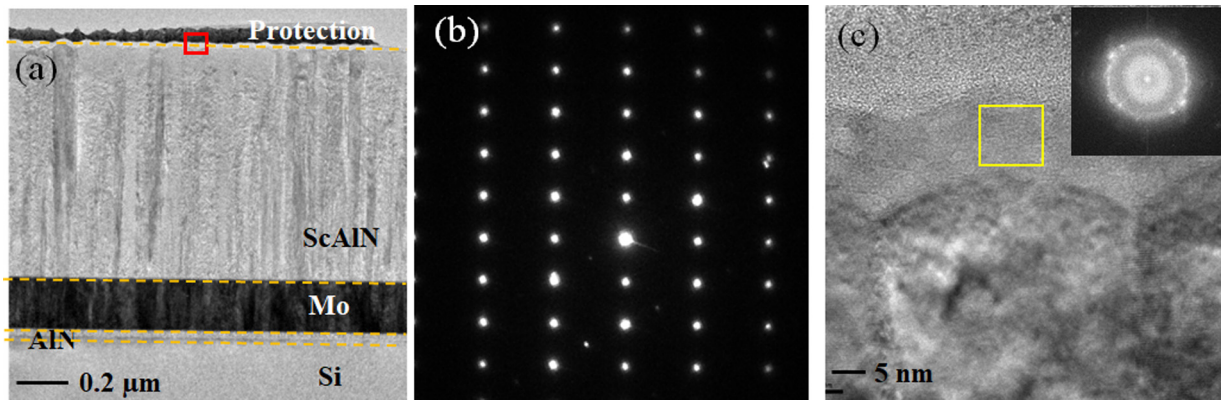

FIG. 1. (a) Cross-sectional TEM overview of the ScAlN/Mo/AlN/Si film stack. The yellow lines are used to guide the film layers. (b) The Selected Area Electron Diffraction (SAED) pattern of the 1 μm thick ScAlN film, demonstrating the good c-axis textured ScAlN film. (c) High-resolution TEM highlights the ScAlN film surface region marked with the red box in (a). The inset shows the FFT pattern reconstructed from the film in the yellow box.

a semiconductor cleanroom environment at about 21 °C and 30%–50% relative humidity. Two months later, the sample was sent for material analyses.

A Transmission Electron Microscope (TEM) equipped with an Energy-dispersive X-ray Spectroscopy (EDX) was used to view the film cross section and characterize the film microstructure and composition. A TEM lamella was prepared by a Focused Ion Beam (FIB) tool. An X-ray Photoelectron Spectroscopy (XPS) with a monochromatized Al Kα x-ray source (1486.6 eV in photon energy) was employed to evaluate the elemental oxidation states and the depth profile of the film stack. The XPS binding energies were calibrated using the C 1s peak at 284.8 eV.

The ScAlN film showed a homogeneous, polycrystalline structure, with columnar grains normally grown to the substrate [Fig. 1(a)]. The Selected Area Electron Diffraction (SAED) pattern indicated that the film grew along the [0002] crystallographic direction [Fig. 1(b)]. High-resolution X-ray diffraction (HRXRD) showed that full width at half maximum (FWHM) of the ScAlN (0002) reflection rocking curve is 1.55° (see the supplementary material, Fig. S1), demonstrating the good *c*-axis textured ScAlN film in the wurtzite crystalline phase.

High-resolution TEM was used to further examine the ScAlN film surface. A thin layer with different image contrast is found between the ScAlN and the lamella protection layer [Fig. 1(c)]. The thickness of this layer is about 10 nm. The Fast Fourier Transformation (FFT) re-constructed the film microstructure in the area marked with the yellow box in Fig. 1(c). The mixed rings and spots displayed on the FFT pattern suggest that both amorphous and small polycrystalline grains co-exist in this region.

Next, the local chemical composition was analyzed using the EDX equipped with the TEM. In the elemental maps of the area indicated by the red box in Fig. 1(a), the scandium, aluminum, and nitrogen were found uniformly distributed throughout the ScAlN bulk film, except on the top surface of the ScAlN film, where a pronounced oxygen signal was detected (Fig. 2). The location and thickness of the region containing oxygen correspond to the partial amorphous layer displayed in Fig. 1(c), confirming that the ScAlN film surface had been oxidized.

XPS core-level spectra were obtained to characterize the chemical state of each element in ScAlN. Using a low power Ar sputtering gun, two kinds of surfaces were prepared for the analysis. The contamination-free oxidized surface and the nonoxidized surface were created by sputtering off the top film surface by 2 and 30 nm, respectively. We found pronounced O 1s peak in the oxidized layer, while the O 1s signal is negligible in the nonoxidized ScAlN [Fig. 3(b)]. By contrast, the N 1s is very weak in the oxidized layer and strong in the nonoxidized ScAlN [Fig. 3(a)]. The binding energies of 530.5 eV for O 1s and 395.7 eV for N 1s agree with those of metal oxide and metal nitride.[24] The Sc 2p binding energies are assignable to Sc $2p_{1/2}$ at the

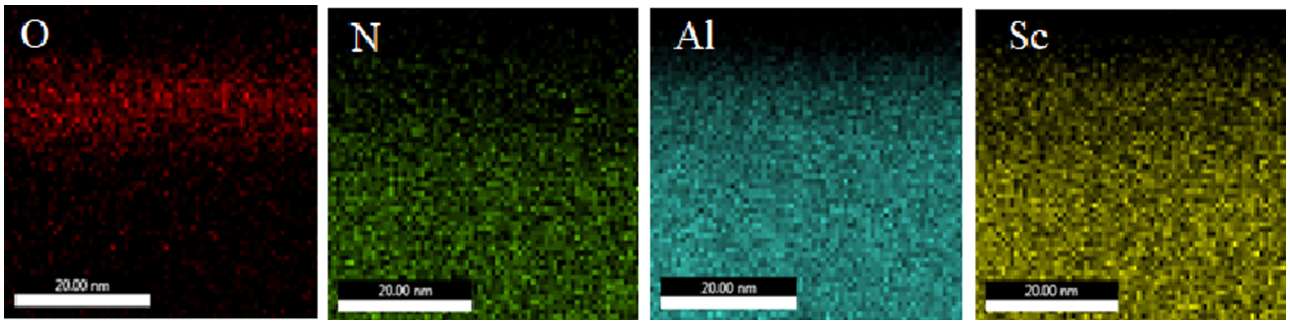

FIG. 2. EDX composition maps in the ScAlN surface region as marked by the red box in Fig. 1(a). Oxide overlayer is revealed on the ScAlN film surface.

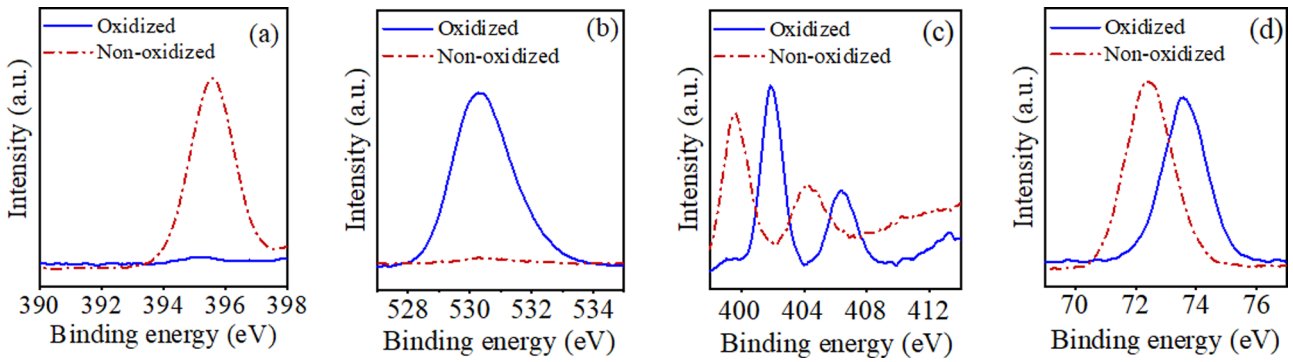

FIG. 3. XPS core-level spectra of (a) N 1s, (b) O 1s, (c) Sc 2p, and (d) Al 2p. Both oxidized and nonoxidized surfaces were recorded for comparison study of formation of metal oxide per oxygen atom measures in the oxygen affinity of a metal atom. As scandium has higher oxygen affinity than aluminum, the formation of the Sc–O bond should be preferred.

higher energy and to Sc $2p_{3/2}$ at the lower energy. In the oxidized layer, both Sc 2p and Al 2p peaks shift to higher energies compared to the nonoxidized film [Figs. 3(c) and 3(d)], reflecting the fact that scandium and aluminum formed stronger bonds with oxygen than with nitrogen. These results suggest that at room temperature, the oxygen in the air chemically reacts with the ScAlN by substituting the nitrogen and bonding with scandium and aluminum atoms. The oxidation mechanism of ScAlN is similar to that of AlN.[19]

The binding between the metals (Sc, Al) and nonmetals (N, O) is analyzed using the bond parameters[25–27] listed in Table I. Thermodynamically, the oxygen substitution of nitrogen in ScAlN is a spontaneous process even at room temperature and atmospheric pressure. The heat of formation of metal oxide per oxygen atom measures the oxygen affinity of a metal atom. As scandium has higher oxygen affinity than aluminum, formation of the Sc-O bond should be preferred.

Due to limited capability for quantitative analysis by TEM-EDX,[28,29] it is difficult to precisely measure the oxygen distribution in the ScAlN film, with oxygen contamination during TEM lamella preparation complicating accurate determination. As a result, we utilized the excellent depth resolution and quantitative capability of XPS to facilitate precise depth evaluation of the oxidation reaction instead. A low power argon gun (1 keV) was used to remove the film surface in stages. After each removal step, the core-level spectra of O 1s, N 1s, Al 2p, and Sc 2p were recorded, and their atomic percentages were calculated. The depth profile plotted with the elemental atomic percentages against sputter time indicates elemental distribution along the direction from the top to the substrate. At the surface of the film (where the sputter time equals to zero), we found high oxygen and low nitrogen amounts (Fig. 4). Toward the substrate, the oxygen amount decreases rapidly to a negligible level and remains at this point thereafter. Conversely, the nitrogen amount increases rapidly. The amounts of nitrogen, aluminum, and scandium remain stable throughout the nonoxidized film, demonstrating the homogeneity of the ScAlN bulk film. The absence of oxygen in the ScAlN film is manifested at about 15 nm away from the surface, corresponding to a sputter time of 5 min. Although the ~6 nm film (corresponding to the sputter time of 3–5 min) contains very low level of oxygen, there is no noticeable contrast in the TEM image and failed in EDX detection. Thus, only the ~10 nm oxide overlayer containing a high concentration of oxygen is observed in Figs. 1 and 2. The higher Sc/(Al + Sc) percentage in the oxide overlayer than that in the bulk film observed in Fig. 4 suggests that composition segregation occurs upon ScAlN surface oxidation.

The absence of oxygen in the ScAlN bulk film indicates that the oxidation reaction is limited to only the film surface in direct contact with air. A self-limiting characteristic also observed in AlN surface oxidation. First principle calculations[20] and *in situ* experiment[12] demonstrated that surface coverage of oxygen dominates the AlN oxidation rate at room temperature. This also suggests that the oxide overlayer formation is chemical reaction controlled. Once the film surface is covered by the newly generated oxide overlayer, direct contact between nitride and oxygen is blocked. Further reaction relies on oxygen diffusion through the oxide overlayer, which is very slow at room temperature and atmosphere pressure.[30] Taking AlN oxidation as a reference, modeling of surface oxidation[12] suggested at room temperature, final oxide thickness and oxidation reaction time constant are about 0.3 nm and 50 s, respectively. Future work is needed to understand the scandium incorporation effect on oxidation kinetics.

We examined the valence band XPS spectra to understand the effect of the oxidation on the electronic structure of the ScAlN film (Fig. 5). The valence band maxima (VBM) were determined by linear extrapolation of the valence band intensity to zero.[31] With ScAlN oxidation, the binding energy of the VBM increases from 0.7 to 2.8 eV. Energy shift was also observed in the oxidation of other nitride materials.[32,33] The higher VBM value indicates a higher energy barrier at

TABLE I. Summary of the bond parameters.

	Sc–O	Sc–N	Al–O	Al–N	Sc	Al
Bond dissociation energy (kJ/mol)[23]	671.4 ± 1.0	464 ± 84	501.9 ± 10.6	≤368 ± 15		
Heat of formation of metal oxide per O (eV)[24,25]					6.7	5.9

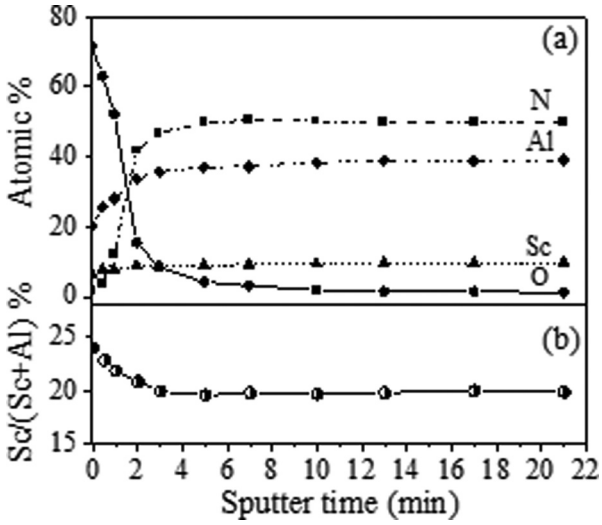

FIG. 4. XPS depth profiles of (a) the atomic percentages of O, N, Sc, and Al. (b) The Sc/(Sc + Al) percentage.

interfaces in the Metal–Insulator–Metal (MIM) structure, which would modulate the charge transportation characteristics of the ScAlN-based piezoelectric and ferroelectric devices.[22,23]

In the oxide overlayer, both aluminum oxide and scandium oxide show very poor piezoelectric behaviors. Surface oxidation, thus, decreases the thickness of the functional film. Because the surface oxidation is self-limited at room temperature, many ScAlN-based piezoelectric and ferroelectric devices work well when the film thickness exceeds several hundred nanometers, given the electronic structure variation at the film surface is taken into consideration. When the film thickness scales down to sub-100 nm, more surface contribution is expected to overall film properties. The changes in film surface composition and structure would lead to additional challenges in device design and integration.

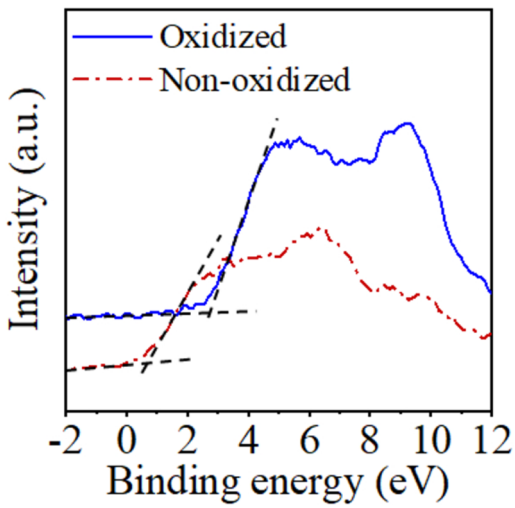

FIG. 5. XPS core-level spectra of the valence band. The VBM values are determined by linear extrapolation of the valence band edge, as illustrated by the dashed lines.

To summarize our findings, we found self-limited oxidation in a *c*-axis textured ScAlN film exposed to air at room temperature. The oxide overlayer formed was 10–15 nm thick, partially amorphous and contained small crystallites. During ScAlN oxidation, the oxygen substitutes the nitrogen, resulting in stronger Al–O and Sc–O bonds and a higher VBM binding energy. Compared to aluminum, scandium has higher oxygen affinity, which enables the Sc–O bond formation to be more energetically favored. Consequently, there would be more scandium in the oxide overlayer than that in the bulk film. The impact of this composition segregation deserves further investigation.

As thinner ScAlN films with a higher scandium content are needed for enhanced electromechanical coupling and in high frequency applications, surface oxidation will pose a greater challenge in these scenarios. Our findings provide an insight to ScAlN surface oxidation, benefiting the design and fabrication of the ScAlN-based electronic devices.

See the supplementary material for HRXRD rocking curve of the ScAlN (0002) reflection.

This work was supported by the Science and Engineering Research Council of A*STAR (Agency for Science, Technology and Research) Singapore, under Grant "Ferroelectric Aluminum Scandium Nitride ($Al_{1-x}Sc_xN$) Thin Films and Devices for mm-Wave and Edge Computing" (No. A20G9b0135).

AUTHOR DECLARATIONS

Conflict of Interest

The authors have no conflicts to disclose.

Author Contributions

Minghua Li: Conceptualization (lead); Data curation (equal); Formal analysis (equal); Investigation (lead); Methodology (lead); Writing – original draft (lead); Writing – review & editing (equal). **Huamao Lin:** Conceptualization (equal); Methodology (equal); Resources (equal); Writing – review & editing (equal). **Kan Hu:** Data curation (equal); Methodology (equal); Writing – review & editing (equal). **Yao Zhu:** Conceptualization (equal); Funding acquisition (lead); Resources (equal); Supervision (equal); Writing – review & editing (equal).

DATA AVAILABILITY

The data that support the findings of this study are available from the corresponding author upon reasonable request.

REFERENCES

[1]S. Zhao, Z. Luo, and T. Wu, IEEE Electron Device Lett. **42**, 1378 (2021).
[2]D. K. T. Ng, C. P. Ho, L. Xu, W. Chen, Y. H. Fu, T. Zhang, L. Y. Siow, N. Jaafar, E. J. Ng, Y. Gao, H. Cai, Q. Zhang, and L. Y. T. Lee, Sens. Actuators, B **346**, 130437 (2021).
[3]N. Wang, Y. Zhu, G. L. Chua, B. Chen, S. Merugu, N. Singh, and Y. Gu, IEEE Electron Device Lett. **40**, 957 (2019).
[4]M. Akiyama, T. Kamohara, K. Kano, A. Teshigahara, Y. Takeuchi, and N. Kawahara, Adv. Mater. **21**, 593 (2009).

[5]K. Frei, R. Trejo-Hernandez, S. Schutt, L. Kriste, M. Prescher, R. Aidam, S. Muller, P. Waltereit, O. Ambacher, and M. Fiederle, Jpn. J. Appl. Phys. **58**, SC1045 (2019).
[6]C. S. Sandu, F. Parsapour, D. Xiao, R. Nigon, L. M. Riemer, T. LaGrange, and P. Muralt, Thin Solid Films **697**, 137819 (2020).
[7]C. Liu, Q. Wang, Y. W. Yang, T. Cao, L. Chen, M. Li, F. Liu, D. K. Loke, J. Kang, and Y. Zhu, in *2021 IEEE International Electron Device Meeting (IEDM), San Francisco, December 11–16* (IEEE, 2021), p. 8.1.1.
[8]M. Akiyama, T. Kamohara, K. Kano, A. Teshigahara, and N. Kawahara, Appl. Phys. Lett. **93**, 021903 (2008).
[9]M. Li, B. Chen, J. Xie, W. Song, and Y. Zhu, in *2020 IEEE International Ultrasonics Symposium (IUS), September 7–11* (IEEE, 2020).
[10]M. Gillinger, M. Schneider, A. Bittner, P. Nicolay, and U. Schmid, J. Appl. Phys. **117**, 065303 (2015).
[11]E. Osterlund, G. Ross, M. A. Caro, M. Paulasto-Krockel, A. Hollmann, M. Klaus, M. Meixner, C. Genzel, P. Koppinen, T. Pensala, A. Zukauskaite, and M. Trebala, Phys. Rev. Mater. **5**, 035001 (2021).
[12]S. Song and F. Placido, Appl. Phys. Lett. **99**, 121901 (2011).
[13]A. Bellucci, S. Orlando, M. Girolami, M. Mastellone, V. Serpente, B. Paci, A. Generosi, A. Mezzi, S. Kaciulis, R. Polini, and D. M. Trucchi, AIP Conf. Proc. **2416**, 020004 (2021).
[14]N. Gungor and M. Alevli, J. Vac. Sci. Technol. A **40**, 022404 (2022).
[15]R. C.Farrell, V. R. Pagan, A. Kabulski, S. Kuchibhatla, J. Harman, K. R. Kasarla, L. E. Rodak, P. Famouri, J. P. Hensel, and D. Korakakis, MRS Online Proc. Library **1052**, 618 (2008).
[16]T. Aubert, J. Bardong, O. Legrani, O. Elmazria, M. B. Assouar, G. Bruckner, and A. Talbi, J. Appl. Phys. **114**, 014505 (2013).
[17]C.-T. Yeh and W.-H. Tuan, J. Adv. Ceram. **6**, 27 (2017).
[18]X. Hou, K.-C. Chou, X. Zhong, and S. Seetharaman, J. Alloys Compd. **465**, 90 (2008).
[19]J. Chaudhuri, L. Nyakiti, R. G. Lee, Z. Gu, J. H. Edgar, and J. G. Wenm, Mater. Charact. **58**, 672 (2007).
[20]Z. Fang, E. Wang, Y. Chen, X. Hou, K.-C. Chou, W. Yang, J. Chen, and M. Shang, ACS Appl. Mater. Interfaces **10**, 30811 (2018).
[21]P. Musavigharavi, A. C. Meng, D. Wang, J. Zheng, A. C. Foucher, R. H. Olsson III, and E. A. Stach, J. Phys. Chem. C **125**, 14394 (2021).
[22]X. Liu, J. Zheng, D. Wang, P. Musavigharavi, E. A. Stach, R. Olsson III, and D. Jariwala, Appl. Phys. Lett. **118**, 202901 (2021).
[23]D. Wang, J. Zheng, P. Musavigharavi, W. Zhu, A. C. Foucher, S. E. Trolier-McKinsky, E. A. Stach, and R. H. Olsson III, IEEE Electron Device Lett. **41**, 1774 (2020).
[24]Y. Matsui, M. Hiratani, Y. Nakamura, I. Asano, and F. Yano, J. Vac. Sci. Technol. A **20**, 605 (2002).
[25]Y. R. Luo, *Comprehensive Handbook of Chemical Bond Energies* (CRC Press, Boca Raton, FL, 2007).
[26]O. Sharia, K. Tse, J. Robertson, and A. A. Demkov, Phys. Rev. B **79**, 125305 (2009).
[27]J. Robertson and Z. Zhang, MRS Bull. **46**, 1 (2021).
[28]D. B. Williams and C. B. Carter, "Quantitative x-ray analysis," in *Transmission Electron Microscopy* (Springer, 1994), Vol. 43, pp. 639–662.
[29]N. Rowlands, E. F. Schumacher, and A. W. Nicholls, Microsc. Microanal. **19**, 1074 (2013).
[30]X. Zhang, P. Zeng, Y. Ma, Y. Jiang, and A. H. Li, Mater. Des. **217**, 110605 (2022).
[31]D. M. Detert, K. B. Tom, C. Battaglia, J. D. Denlinger, S. H. N. Lim, A. Javey, A. Anders, O. D. Dubon, K. M. Yu, and W. Walukiewicz, J. Appl. Phys. **115**, 233708 (2014).
[32]A. M. Shing, Y. Tolstova, N. S. Lewis, and H. A. Atwater, Appl. Phys. A **123**, 735 (2017).
[33]V. A. Gritsenko, A. V. Shaposhnikov, W. M. Kwok, H. Wong, and G. M. Jidomirov, Thin Solid Films **437**, 135 (2003).